RSC Applied Interfaces

ROYAL SOCIETY OF CHEMISTRY

PAPER

View Article Online
View Journal | View Issue

Cite this: *RSC Appl. Interfaces*, 2026, 3, 69

Chalcopyrite–quartz mineral surfaces: controlled wetting and spreading by xanthate-tallow diamine emulsions

Azeez G. Aregbe,[ab] Wei Sung Ng,[ab] Tina Hsia,[bc] Anton Blencowe,[be] Alireza Allahyari,[bd] Marta Krasowska,[bd] San H. Thang[bc] and George V. Franks *[ab]

This study investigated emulsions formulated with water-soluble xanthates, including potassium amyl xanthate (PAX) and a novel α-tocopherol polyethylene glycol 400 succinate xanthate (TPGS-X), combined with oil-soluble *N*-hydrogenated tallow-1,3-propylene diamine (tallow diamine). The emulsion droplets were examined for selective attachment and controlled oil spreading onto homogeneous and heterogeneous chalcopyrite–quartz mineral surfaces, with particular focus on targeting chalcopyrite regions over pure quartz surfaces. The stability and characteristics of kerosene-in-water emulsions containing xanthate and tallow diamine were studied across different pH values, examining both mostly protonated and deprotonated states of the tallow diamine. The emulsions became unstable when tallow diamine was mostly protonated due to electrostatic interactions between the cationic tallow diamine and anionic xanthates resulting in near zero zeta potentials. Conversely, the emulsions exhibited relative stability when tallow diamine was mostly deprotonated and the droplets were stabilised by negatively charged xanthates at the interface. Under these stable conditions, TPGS-X demonstrated superior performance compared to PAX, with the higher molecular weight enhancing emulsion stability. Oil contact angle measurements revealed that oil preferentially wetted chalcopyrite over quartz when the oil-soluble emulsifier was mostly deprotonated, but wetted both minerals when tallow diamine was mostly protonated. Similarly, oil droplets selectively wetted chalcopyrite patches *via* xanthate interactions when tallow diamine was mostly deprotonated, but subsequently spread onto quartz surfaces of heterogeneous minerals when tallow diamine became mostly protonated. These findings demonstrate the potential for applying oil-containing hydrophobicity modifiers to achieve selective oil attachment and controlled spreading onto composite chalcopyrite–quartz minerals. This approach offers promising opportunities for selective recovery of chalcopyrite over coarse quartz mineral particles through pH-controlled emulsion behaviour and targeted surface interactions.

Received 15th September 2025,
Accepted 29th September 2025

DOI: 10.1039/d5lf00275c

rsc.li/RSCApplInter

Introduction

Wetting and spreading are fundamental phenomena in several industrial applications, including lubrication, coating, printing, enhanced oil recovery, and froth flotation.[1–6] A typical example is the attachment and spreading of an oil droplet on a solid substrate, displacing water or other immiscible solutions from the surface.[2,7,8] Studies have shown that the surface wettability of a material can be altered through various methods such as light irradiation, thermal treatment, application of an electric field, and solvent treatment.[9–13] Moreover, the ability of a liquid to wet and spread on a surface is crucial for bubble or droplet-surface attachment in many processes, particularly froth flotation. Generally, when materials contact each other, molecular interactions result in adhesive forces (between materials) and cohesive forces (within materials). Adhesive forces between the solid and liquid promote wetting, while cohesive forces within the liquid resist it. The balance between these forces determines the surface wettability.

Contact angle is commonly used to quantify wetting on a solid surface. It is influenced by the surface energies of the phases in contact.[14] The contact angle of water on a surface

[a] *Chemical Engineering, University of Melbourne, Parkville, VIC 3010, Australia. E-mail: gvfranks@unimelb.edu.au*
[b] *ARC Centre of Excellence for Enabling Eco-efficient Beneficiation of Minerals, Australia*
[c] *School of Chemistry, Monash University, Clayton Campus, VIC 3800, Australia*
[d] *Future Industries Institute, University of South Australia, UniSA STEM, Mawson Lakes, SA 5095, Australia*
[e] *Applied Chemistry and Translational Biomaterials (ACTB) Group, Centre for Pharmaceutical Innovation (CPI), UniSA Clinical and Health Sciences, University of South Australia, Adelaide, SA 5000, Australia*

indicates its hydrophobic or hydrophilic nature: an angle over 90° signifies hydrophobicity (low affinity for water or high affinity for air and oil), whereas an angle below 90° indicates hydrophilicity (high affinity for water or low affinity for air and oil).[15,16] At equilibrium, Young's equation provides a unique contact angle for a given system, as shown in eqn (1).

$$\cos\theta = \frac{\gamma_{SF} - \gamma_{SL}}{\gamma_{LF}} \quad (1)$$

where γ_{SF}, γ_{SL}, and γ_{LF} represent the interfacial tension (IFT) at the solid–fluid (either gas or another immiscible liquid), solid–liquid, and liquid–fluid interfaces, respectively.

The attachment and spreading of an oil droplet on a solid surface in an aqueous system is a liquid–liquid displacement process. When the liquid oil droplet approaches the surface, there is the formation of a three-phase contact line after the thin film ruptures. This is followed by its expansion and the spreading of the oil molecules over the surface with the displacement of adjacent water molecules. This spreading continues until the oil droplet achieves an equilibrium contact angle.

In many industrial processes, including froth flotation, the application of surfactants is used to control wettability and spreading. Flotation is a physicochemical process that involves the separation of valuable minerals (such as chalcopyrite or copper minerals) from gangue or waste materials (such as quartz or clays), based on differences in surface wettability.[17] It strongly depends on an effective bubble–particle attachment and the transfer of the particle–bubble aggregates to the froth layer for mineral recovery.[18] To enhance the difference in the surface hydrophobicities of the valuable and gangue minerals, selective surfactants, such as xanthates are used for sulfide ores.

However, the flotation process is mainly effective for particle diameters between 20 to 150 μm.[19–21] Fine particles smaller than 20 μm have low recoveries due to poor bubble–particle collision efficiency.[22,23] On the other hand, the recovery of coarse particles with diameters above 150 μm is low due to high particle–bubble detachment caused by turbulence in the flotation cell.[24–26] The detachment of coarse particles is particularly problematic for composite/heterogeneous particles exhibiting multiple types of minerals on the surface, as only a small portion of the particle surface is usually hydrophobic. This is associated with reduced probabilities for particle–bubble contact to result in attachment. Furthermore, any resulting attachment with this small surface area is often not enough to form a stable bubble–particle aggregate due to reduced adhesion strength.

Despite these challenges, coarse particle flotation is desirable as it offers various benefits. Froth flotation at coarser sizes will lead to the early rejection of gangue or waste materials. This will reduce the water and energy consumption for subsequent grinding of ore samples to suitable particle sizes for optimum recovery. The development of new flotation cells based on fluidized-bed technologies (including HydroFloat™ and NovaCell™)[27,28] has been used to reduce turbulence and improve coarse particle recovery. Other researchers have focused on more advanced hydrophobicity modifiers (such as emulsions and collectors)[29–32] to increase bubble–particle adhesion. Thus, an innovative chemical approach for conventional coarse particle flotation is required to address these issues.

Moreover, coarse particles have an increased tendency to be present as composites containing both gangue and valuable minerals, as the valuable mineral is generally not liberated at coarse sizes, especially for low-grade, finely-disseminated ores. It can be challenging to sufficiently hydrophobize composite coarse particles as the exposed surface areas might contain a low fraction of valuable minerals. As the valuable minerals are generally targeted for selective attachment by surfactants currently used in flotation, this effectively reduces the hydrophobic surface area available for particle–bubble attachment. Hence, for these coarse composites, recovery may remain poor, and it is critical to develop methods for targeting and modifying such particles.

In this work, we propose a novel system comprising an oil-in-water emulsion with two different surfactants for coarse composite chalcopyrite–quartz particle flotation, as illustrated in Fig. 1. The first surfactant is a water-soluble collector for the selective attachment of the oil droplet to the valuable mineral such as chalcopyrite (*i.e.*, xanthates), whereas the second surfactant is tallow diamine (abbreviated as "tallow" in the figures for simplicity) known to enhance the spreading of the oil droplet onto the quartz surface when the tallow diamine is mostly protonated.[33–35] The motivation for selecting the xanthate surfactants is that they are the common collectors for chalcopyrite flotation.[30,31] They are known to increase the surface hydrophobicity of chalcopyrite.[36–38] Tallow diamine was chosen because of its wide applications for oil spreading on siliceous materials in road pavement.[34,35] *N*-Hydrogenated tallow-1,3-propylene diamine (or tallow diamine) with ammonium functional groups possesses a positive charge in acidic conditions. In contrast, tallow diamine is mostly deprotonated in alkaline conditions above its pK_a.[39,40] The pK_a values of the two amines were determined by potentiometric titration to be pK_{a1} ≈ 9.8 and pK_{a2} ≈ 7.7 as presented in the SI section (Fig. S1). At pH 11, this corresponds to a tallow diamine fractional charge of +0.06, which we refer to as mostly deprotonated, while at pH 9, the fractional charge is about +0.91, which we refer to as mostly protonated. Tallow diamine is known to alter the surface characteristics of negatively charged siliceous oxide minerals, such as quartz, from hydrophilic to hydrophobic[34,35] when the pH is below its pK_a values.

Targeted spreading

To the best of our knowledge, there are no studies in the open literature on the application of oil-containing hydrophobicity modifiers containing xanthates and tallow diamine for improving the hydrophobicity of composite chalcopyrite–quartz mineral surfaces for the potential application for coarse particle

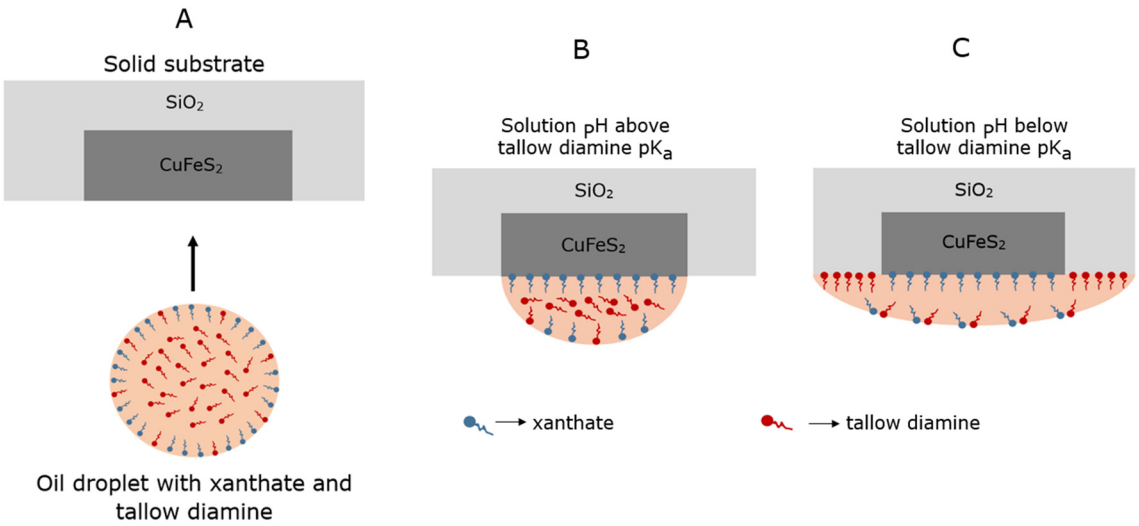

Fig. 1 The proposed concept for the attachment and spreading of an oil droplet containing hydrophobicity modifiers from a chalcopyrite ($CuFeS_2$) patch to a quartz surface. A. The collision of the oil droplet containing xanthate and tallow diamine with the composite mineral, at a pH value above the pK_a of tallow diamine (where it is mostly deprotonated). B. Oil droplet attachment to and wetting of the chalcopyrite surface *via* xanthate surfactant at pH values above the tallow diamine pK_a. C. Oil droplet wetting and spreading to the quartz surface as the solution pH is decreased below the pK_a of tallow diamine, where it becomes positively charged, and adsorbs onto the quartz surface.

flotation. With this proposed system, the xanthate molecules will enable the droplets to selectively target the coarse composites containing the valuable mineral and droplet attachment to such a surface. After that, the tallow diamine will enable oil spreading beyond the boundary of the valuable mineral, promoting oil coverage over an area of the coarse particle that is larger than the patch of valuable mineral, and hence improving the ability and probability of the particle to be attached to an air bubble and be recovered by froth flotation. Importantly, the targeting ability of xanthate helps distinguish between coarse composite particles containing chalcopyrite from those containing only quartz.

In order to deliver oil droplets to mineral particle surfaces, a stable emulsion was formulated at a pH above the highest pK_a of the tallow diamine (pK_{a1} ≈ 9.8 and pK_{a2} ≈ 7.7), where it is mostly deprotonated. Xanthates (which are negatively charged and amphiphilic at high pH values) were used to stabilize the emulsion, as published recently.[41] The oil/water interface becomes negatively charged due to the adsorption of the charged xanthate surfactants on the surface. As shown schematically in Fig. 1A, the oil droplet with xanthate and tallow diamine interacts with the polished composite mineral surface at pH values above the pK_a of the tallow diamine. The selective attachment of the oil droplet to the exposed chalcopyrite parts of the surface is *via* the xanthate, which is well known to selectively adsorb to copper sulfide mineral surfaces,[42,43] as depicted in Fig. 1B. The oil wets and spreads only on the copper sulfide surface, $CuFeS_2$. Although the tallow diamine is surface active, it is mostly deprotonated and does not contribute to the surface charge on the droplets at pH values above its pK_a.

However, when the solution pH is changed to below its pK_a, the tallow diamine becomes mostly protonated (positively charged) and amphiphilic. It can then enable the oil droplet to wet and spread to the quartz surface as the positively charged tallow diamine will adsorb on negatively charged quartz, as shown in Fig. 1C. Some tallow diamine molecules will adsorb at the oil–water interface, resulting in a change in the electric state of this interface with the negative charge at the oil–water interface being reduced in magnitude/close to neutral. The deposited oil layer is expected to spread from a small chalcopyrite patch to cover the entire surface of the composite particle, including the quartz.

Prior to the application of the proposed system for coarse particle flotation, it is crucial to understand how the interaction between the xanthate and tallow diamine influences the emulsion stability when the latter is mostly protonated or deprotonated. Furthermore, the droplet attachment and spreading of oil-solubilized hydrophobicity modifiers on chalcopyrite and quartz surfaces should be investigated. Therefore, in this study, the stability and characterization of kerosene-in-water emulsions formulated with xanthates and tallow diamine at pH values below and above the pK_a of tallow diamine were investigated. Subsequently, the oil contact angles on chalcopyrite and quartz mineral surfaces in the presence of xanthates and tallow diamine at pH values below and above the pK_a of the tallow diamine were studied.

The commercially available flotation collector, potassium amyl xanthate (PAX), was used as the baseline surfactant because it is the longest chain xanthate currently used in the mineral processing industry.[44,45] Its performance was compared with a novel α-tocopherol polyethylene glycol 400 succinate xanthate (TPGS-X) surfactant. The novel reagent has previously been found to improve the stability of the formulated emulsions in comparison with PAX, as reported in our recently published paper.[41] The novel xanthate had

the slowest creaming rate due to its chemical structure, molecular weight, and hydrophilic–lipophilic balance.[41] Moreover, the novel xanthate was synthesized from vitamin E as an environmentally-friendly and cost-efficient raw material. It is also an improved collector for chalcopyrite flotation compared to PAX.[46]

Materials and methods

Reagents and mineral samples

Potassium chloride (KCl; analytical reagent (AR) grade, ≥99%), ethanol (AR grade, ≥99%), and isopropanol (AR grade, ≥99%) were purchased from ChemSupply (Australia). Sodium hydroxide (NaOH; AR grade, ≥ 99%) was supplied by Merck KGaA (Australia), and hydrochloric acid (HCl; AR grade, ≥38%) was obtained from Scharlau (Australia). Potassium amyl xanthate (PAX; AR grade, ≥97%) was purchased from Tokyo Chemical Industry Co. Ltd (Japan), and *N*-hydrogenated tallow-1,3-propylene diamine (tallow diamine; high grade) was supplied by Shandong Xin Guang Chemistry Co. Ltd (China). Pieces of pure chalcopyrite (assayed grade >98%) and pure quartz (assayed grade >98%) were obtained from Geo Discoveries (Australia), and the composite mineral pieces were supplied by Distinction Crystals & Fossils (United Kingdom). Kerosene (AR grade, ≥99%) was purchased from Sigma-Aldrich (Australia). These reagents were used as received without further purification. TPGS-X was synthesized as described previously[41] and has the same head group area as conventional xanthates such as PAX. Potassium chloride (0.01 M) was used as the background electrolyte. The pH modifiers used are hydrochloric acid (1 M) and sodium hydroxide (1 M). Reverse osmosis (RO) water (resistivity = 1.2 MΩ cm) was used throughout the experiment for cleaning and preparing the aqueous solutions. The photographs of the polished mineral samples used for the contact angle measurements are shown in Fig. 2.

Interfacial tension measurements

A profile analysis tensiometer PAT1-M (SINTERFACE Technologies, Germany) was used to measure oil–water interfacial tension (IFT) both in the absence and presence of surface-active species (*i.e.*, PAX, TPGS-X, and tallow diamine). The tensiometer was mounted on an anti-vibration table (Vision IsoStation, Newport, USA) to minimise environmental vibration effects. The temperature within the quartz cuvette was controlled by a computer-controlled external circulating bath (Julabo, Germany) with ±0.03 °C resolution and monitored *via* a temperature probe immersed in the cuvette. Once the aqueous phase reached the desired temperature, oil was delivered through the PTFE tubing system using a 100 μL gastight syringe (ILS®, Germany) until a droplet of known and constant volume (14 μL) formed at the tip of a U-shaped stainless steel capillary with an outer diameter of 2 mm (SINTERFACE Technologies, Germany). The interfacial tension was determined through fitting the silhouette of the droplet with the Young–Laplace equation. Emulsifier adsorption kinetics were monitored until steady state was established, defined as an interfacial tension change of 0.1 mN m^{-1} or less over 1000 s. All experiments were conducted at 22 ± 1 °C in triplicate. Due to the high surface activity of tallow diamine, a smaller capillary was required to balance the low interfacial tension with droplet stability at the capillary tip. A pendant-drop configuration was therefore employed, using a straight capillary with an outer diameter of 0.5 mm to generate an aqueous droplet with a constant area of 2 mm^2 in a cuvette containing the oil phase. For all experiments, the profile-fitting error when fitting the droplet silhouette to the Young–Laplace equation was less than 1 μm.

The IFT measurements were conducted with similar concentrations of xanthates and tallow diamine as those in the emulsion formulation and contact angle studies at pH values when the tallow diamine is mostly protonated (pH 9) and deprotonated (pH 11). The following IFT measurements were taken at both pH 9 and 11:

a) IFT of kerosene in water containing 0.01 M KCl in the absence of surface-active species.

b) IFT of kerosene in aqueous xanthate solutions (1.8 mM PAX or 0.03 mM TPGS-X).

c) IFT of kerosene containing 0.86 mg g^{-1} tallow diamine in water containing 0.01 M KCl.

d) IFT of kerosene containing 0.86 mg g^{-1} tallow diamine in aqueous xanthate solutions (1.8 mM PAX or 0.03 mM TPGS-X).

Emulsion formulation and characterization

An aqueous solution containing 0.01 M KCl was used throughout the experiment and is referred to as the aqueous solution in this paper, with KCl present as the background electrolyte. The emulsion was formulated with a kerosene : water mass ratio of 1 : 3 to create an oil-in-water emulsion

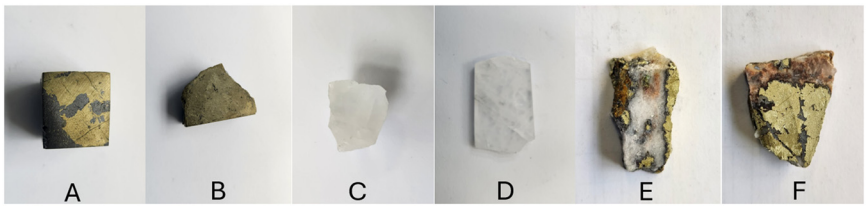

Fig. 2 Photographs of the mineral samples for oil contact angle measurements: A. and B. pure chalcopyrite samples; C. and D. pure quartz samples; E. and F. composite chalcopyrite–quartz samples.

and to deposit an oil layer on the mineral surface. The dosages of the emulsifiers were also calculated based on the oil volume in the emulsion. The masses of the xanthate surfactants (*i.e.*, PAX and TPGS-X) required to form an emulsion with an average size of 10 μm were calculated using their head group areas and molecular weights (PAX = 202 g mol^{-1} and TPGS-X = 1069 g mol^{-1}), as previously reported.[41] The calculated masses were 0.11 g PAX and 0.55 g TPGS-X, which were dissolved in 300 g of aqueous solution.

PAX and TPGS-X exhibit different solubilities in water, which are also indicated by their hydrophilic–lipophilic balance (HLB) values of ≈12.9 and 9.1, respectively (estimated with Griffin's equation).[41,47] Based on the differences in solubilities, the aqueous solution of PAX was left at room temperature for 1 h for complete dissolution, while the aqueous solution of TPGS-X was stirred and heated at 50 °C for 1 h. Moreover, two aqueous solutions were prepared for each surfactant. The first solution had a pH value below the pK_a of tallow diamine, whereas the second solution had a pH value above the pK_a of tallow diamine. The first solution pH was not modified (with a pH of ≈6.6 for PAX and 8.1 for TPGS-X), but the second solution pH was adjusted with NaOH (1 M) to a pH of ≈12.0 for PAX and 11.8 for TPGS-X.

The tallow diamine is oil-soluble[48] with an average molecular weight of 319 g mol^{-1} (estimated from ^{1}H NMR analysis as described in Fig. S2–S7 of the SI section) and an HLB of ≈2.0 (estimated from the chemical composition (Fig. S8)[49,50] and Griffin's equation). The detailed analysis and calculation are provided in the SI section. An equimolar ratio with PAX was used to calculate the tallow diamine mass required for the emulsification process. Then, the calculated mass (≈0.086 g of tallow diamine) was dissolved in 100 g kerosene. The kerosene-surfactant solution was stirred and heated at 50 °C for 1 h. After cooling to room temperature, the kerosene and aqueous solutions were mixed and homogenized with a high-speed mixer (IKA Ultra Turrax T45; Janke and Kunkel GmbH; Germany) at 9600 rpm for 10 min. Next, the kerosene-in-water emulsion characteristics, such as droplet size, Zeta potential, creaming rate, and oil separation, were investigated. The droplet size distributions were measured with a Mastersizer 3000 laser diffraction particle size analyzer (Malvern Panalytical, United Kingdom), and examined under an optical microscope (BX51; Olympus, Japan). Additionally, the emulsion pH was measured with a pH meter (LAQUA-PH1300; Horiba Scientific, Japan) within 6 min after emulsification. Subsequently, the zeta potentials of the kerosene-in-water emulsions were determined using a ZetaProbe analyzer (Colloidal Dynamics, Australia) at a constant ionic strength of 0.01 M KCl. The oil separation and creaming rates of the emulsions were also studied for 100 h at ambient temperature conditions in a 500 mL graduated cylinder as described previously.[41]

Contact angle measurements

Different concentrations of PAX (0.18 and 1.8 mM) and TPGS-X (0.01 and 0.03 mM) were prepared with an aqueous solution containing 0.01 M KCl. The tallow diamine was prepared by dissolving 0.086 g of tallow diamine in 100 g of kerosene. Subsequently, the mineral pieces were cut with a Struers cutting machine (Accutom-50, Denmark) and polished with silicon carbide papers (diameter ≈250 mm and grain size ≈22 μm) to remove any irregularities, refresh the surface, and obtain a flat surface for contact angle measurements (Fig. 2). Then, the samples were cleaned with isopropanol, ethanol, and water, and dried under nitrogen prior to the contact angle measurement.

The captive droplet method was used for the experiment to measure the static contact angles on mineral surfaces using an optical contact angle measuring instrument (Dataphysics OCA 20, Germany). The schematic diagram of the experimental set-up is provided in Fig. S9. Firstly, the U-shaped stainless steel needle (outer diameter of 0.2 mm) was connected to the syringe and filled with pure kerosene. Then, the needle-syringe set-up was attached to the Dataphysics OCA20 instrument. The optical glass cuvette was filled with a solution containing the desired aqueous phase. This was followed by the attachment of the polished and cleansed mineral to the glass slide with adhesive. The measurements were conducted at room temperature (approximately 20 °C). For each experimental run, eight data points were measured at different spots on the polished mineral surface.

For each measurement, the oil phase was gradually dispensed from the needle until the droplet volume reached approximately 30 μL. Then, the droplet was allowed to detach from the needle and approach the mineral surface. Afterward, the oil contact angle on the mineral surface was measured between 10 and 60 s after contacting the surface. Between measurements, the beaker was cleaned with RO water, ethanol, and isopropanol (three times) and dried under nitrogen, while the solid substrate was polished and cleaned. For the baseline studies with no surfactant, the oil phase was kerosene, while the aqueous phase was 0.01 M KCl solution. This was conducted only on the pure mineral samples.

For the measurements with only xanthate surfactants, the oil phase was kerosene, while the aqueous phase consisted of the studied xanthates at different concentrations (0.18 and 1.8 mM of PAX, and 0.01 and 0.03 mM of TPGS-X) in 0.01 M KCl solution. The xanthate solutions were prepared and used within 3 h after preparation, as xanthates can decompose in aqueous solutions with time.[51] The pH value of the aqueous xanthate solution was not modified in this measurement, so the pH value was approximately 6.6 for PAX and 8.1 for TPGS-X. In these experiments, it was assumed that the surfactants in solution migrate to the oil–water interface almost instantaneously as they are surface active, so that by the time the droplet contacts the solid surface, both the solid and droplet have xanthate surfactant on their surfaces. Measurements with only xanthate were conducted only on the pure mineral samples.

For the measurements of contact angle with both xanthate (present in solution and on the surface of the drop) and tallow diamine, the xanthate solutions were prepared as

described previously as the aqueous phase, while 0.86 mg g^{-1} tallow diamine in kerosene solution was used as the oil or drop phase. Three sets of measurements were conducted with the xanthate and tallow diamine system. The first set was performed at pH 11, above the higher pK_a of tallow diamine (fractional charge about +0.06), while the second set was performed at pH 9, between the pK_as of tallow diamine (fractional charge about +0.91). These first two sets were conducted with the pure chalcopyrite (A and B) and quartz (C and D) minerals. The third set of measurements featured a pH change from pH 11 to pH 9, and was conducted with the pure chalcopyrite (A and B) and the composite (E and F) minerals.

The third set was conducted with the aqueous phase initially at pH 11. For this set, after the oil phase droplet was dispensed from the needle and present on the mineral surface, a few drops of 1 M HCl were added to reduce the pH of the aqueous phase to below the pK_a of tallow diamine. This was expected to protonate the tallow diamine and enable the oil droplet to spread to the quartz surface on the composite mineral, thereby increasing oil coverage and enhancing the hydrophobicity of the composite mineral surface. In addition to the measurement of the contact angle before and after the pH change, videos were taken documenting the spreading of the oil. The third set was also conducted on the pure chalcopyrite mineral for comparison to confirm that the change in pH only caused spreading onto quartz but not onto chalcopyrite.

Results and discussion

Interfacial tension measurements

The interfacial tension measurements are helpful in understanding under which conditions the xanthates and tallow diamine are found to be surface active, which tends to segregate to the oil–water interface and reduce the interfacial tension. The results are presented in Fig. 3. The interfacial tension between kerosene and water is between 46 and 48 mN m^{-1} at pH 11 and 9, respectively, consistent with the literature.[52–54] PAX is slightly surface active and reduces the interfacial tension by about 1 to 2 mN m^{-1} at 1.8 mM concentration. This is consistent with the relatively short hydrocarbon chain of PAX and its high solubility in water. In contrast, TPGS-X is more effective in reducing the interfacial tension to 22 and 29 mN m^{-1} at pH 9 and 11, respectively, indicating that it is present at the oil–water interface at both pH values. This indicates that TPGS-X is at the surface of the oil droplets. Surprisingly, the interfacial tension when tallow diamine is present is significantly lower at around 1–2 mN m^{-1} at both pH 9 and 11. This shows that the tallow diamine is present at the interface at both pH values, independent of whether it is mostly protonated or deprotonated.

Moreover, as discussed in the subsequent sections, the tallow diamine did not improve the emulsion stability when it was mostly deprotonated. The emulsion separated into its oil and water phases immediately after the emulsification process,

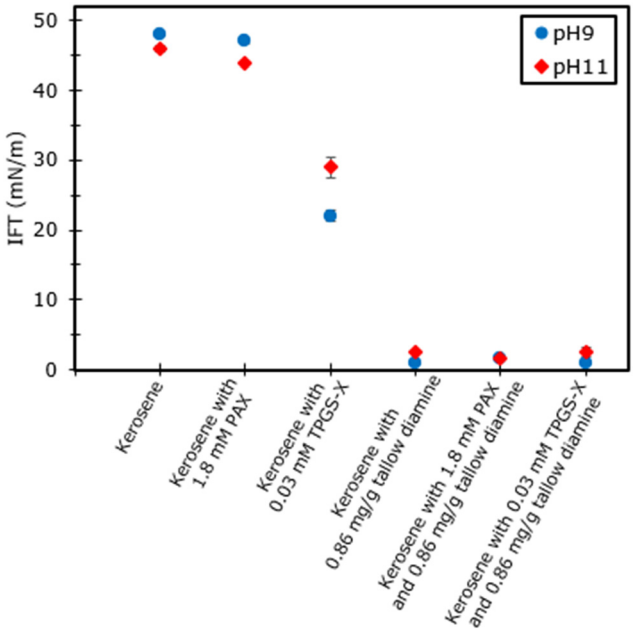

Fig. 3 Steady state interfacial tension values 1000 s after formation of the droplet. Values are the mean and standard deviation of (n = 3) measurements.

which is similar to the behavior of the emulsion without any surfactant. Furthermore, the mostly deprotonated tallow diamine did not promote oil spreading on pure quartz, and the oil contact angle of kerosene containing tallow diamine is similar to that of pure kerosene. This suggests that it is mostly deprotonated, though it is at the oil–water interface. However, the mostly protonated tallow diamine improved the emulsion stability and promoted oil spreading on quartz because its amine groups become positively charged when the surfactant is mostly protonated.

Emulsion characterization and stability

Prior to the emulsification studies, the pH values of the aqueous solutions and kerosene-in-water emulsions were measured to investigate any potential variation in pH during the emulsification process. This is important to understand if there is a significant change in pH during emulsification under conditions above the pK_a of tallow diamine. The zeta potentials of the emulsions were also determined at a constant ionic strength of 0.01 M KCl. The results are shown in Table 1. The pH of the final emulsions did not vary substantially from the pH of the starting solutions. For example, below the pK_a of tallow diamine, the emulsion and solution pH values were 6.6 and 7.4 for PAX, and 8.1 and 8.0 for TPGS-X, respectively. Similarly, above the pK_a of tallow diamine, the emulsion and solution pH values were 12.0 and 11.5 for PAX, and 11.8 and 11.7 for TPGS-X, respectively.

The zeta potentials of the emulsions were useful to understand the interaction between the tallow diamine and xanthates under conditions where the tallow diamine was

Table 1 Zeta potentials (mV) and pH values of the emulsions with xanthates and tallow diamine at a constant ionic strength of 0.01 M KCl

System	PAX with tallow diamine < pK_a	PAX with tallow diamine > pK_a	TPGS-X with tallow diamine < pK_a	TPGS-X with tallow diamine > pK_a
Solution pH	6.6	12.0	8.1	11.8
Emulsion pH	7.4	11.5	8.0	11.7
Emulsion zeta potential (mV)	0	−45	−2	−68

either mostly protonated (positively charged) or deprotonated (Table 1). When the pH was below the pK_a of the tallow diamine, protonation of the amine resulted in the formation of an ion pair with the negatively charged xanthate. This reduced the availability of charged ions on the surface of the emulsion droplet, and the resulting surface potential on the droplets became close to zero (*i.e.*, emulsion zeta potentials of 0 mV for PAX and −2 mV for TPGS-X with tallow diamine at pH below its pK_a). However, when the pH was above the pK_a and the tallow diamine was mostly deprotonated, the emulsions exhibited relatively high negative zeta potential values (*i.e.*, emulsion zeta potentials of −45 mV for PAX and −68 mV for TPGS-X). These values were close to the results obtained from the emulsions with only xanthates as emulsifiers.[41] This shows that the emulsions can be stabilized by the xanthates at the oil–water interface when the tallow diamine is mostly deprotonated and does not neutralize the xanthate.

The droplet size distributions of the kerosene-in-water emulsions were measured *via* laser diffraction (Fig. 4) and observed with optical microscopy (Fig. 5). The emulsions formulated at pH values above the pK_a of the tallow diamine are characterized by smaller droplet diameters, similar in size to those reported for the emulsions with only xanthates as emulsifiers.[41] This is due to the tallow diamine being mostly deprotonated at pH above its pK_a. Under these conditions, the emulsion is stabilized solely by xanthate molecules at the kerosene–water interface, with coalescence being prevented by the high negative zeta potential values. The size distributions of the kerosene-in-water emulsions at pH values above the pK_a of tallow diamine are similar to those reported for the emulsions with only xanthates as emulsifiers.[41]

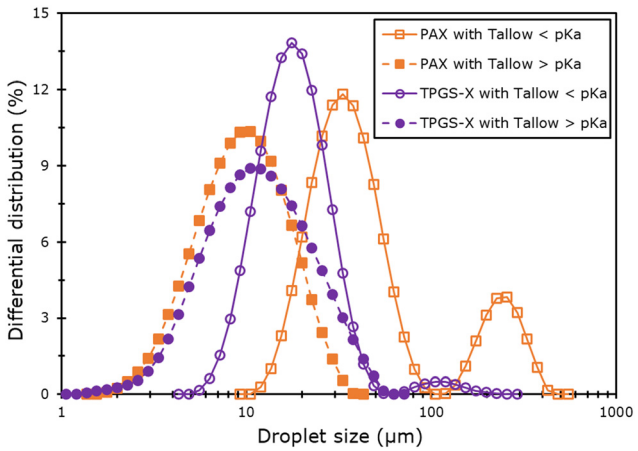

Fig. 4 Droplet diameter distributions in kerosene-in-water emulsions within 6 min after the emulsification. PAX with tallow diamine < pK_a (open squares-orange) and PAX with tallow diamine > pK_a (filled squares-orange) indicate the emulsions with PAX and tallow diamine at pH below and above the pK_a of tallow diamine, respectively. TPGS-X with tallow diamine < pK_a (open circles-purple) and TPGS-X with tallow diamine > pK_a (filled circles-purple) show the emulsions with TPGS-X and tallow diamine at pH values below and above the pK_a of tallow diamine, respectively.

Moreover, the kerosene-in-water emulsions at pH values below the pK_a of tallow diamine have larger droplet diameters compared with the emulsions at pH values above the pK_a of tallow diamine. This result indicates that the oil-soluble surfactant interacts with the anionic surfactant when it is mostly protonated (charged) at pH below its pK_a. The close to 0 mV zeta potential values indicate that the oppositely charged surfactants likely neutralize each other. As such, they will be less effective in stabilizing the emulsion droplets because the near-zero zeta potential will not lead to any significant EDL repulsion between droplets. The images in Fig. 5 confirm that the emulsions coalesce and coarsen at pH values below the pK_a of the tallow diamine compared to above the pK_a.

The oil phase separation and creaming rates of the kerosene-in-water emulsions at pH values below and above the oil-soluble surfactant pK_a were studied for 100 h. The photographic images of the emulsions with PAX and tallow diamine, as well as the emulsions with TPGS-X and tallow diamine after 10 and 100 h are shown in Fig. S10 and S11, respectively, in the SI section. The figures show that after 10 h, the emulsions at pH below the pK_a of tallow diamine exhibit a near-complete phase separation. This suggests that the interaction between the negatively and positively charged surfactant molecules at the oil–water interface leads to a negligible/neutral zeta potential (−2 to 0 mV) at the droplet surface. Considering the very small magnitude of the zeta potential and high ionic strength of the aqueous phase (0.01 M KCl, Debye length of ~3 nm), the resulting electrical double layer (EDL) forces will be weak and short-range, hence not being able to inhibit/prevent coalescence.

Moreover, the images of the emulsions containing only the tallow diamine before and after tallow diamine protonation for 1 and 10 h are reported in Fig. S12. The figures indicate that the emulsion was very unstable when the tallow diamine was mostly deprotonated, which is similar to the observation with the kerosene-in-water emulsion without any emulsifier, as reported in our previous paper.[55] On the other hand, the emulsion was relatively stable when the tallow diamine was mostly protonated because it acted as the emulsifier and improved the stability of the emulsion (Fig. S12). This indicates

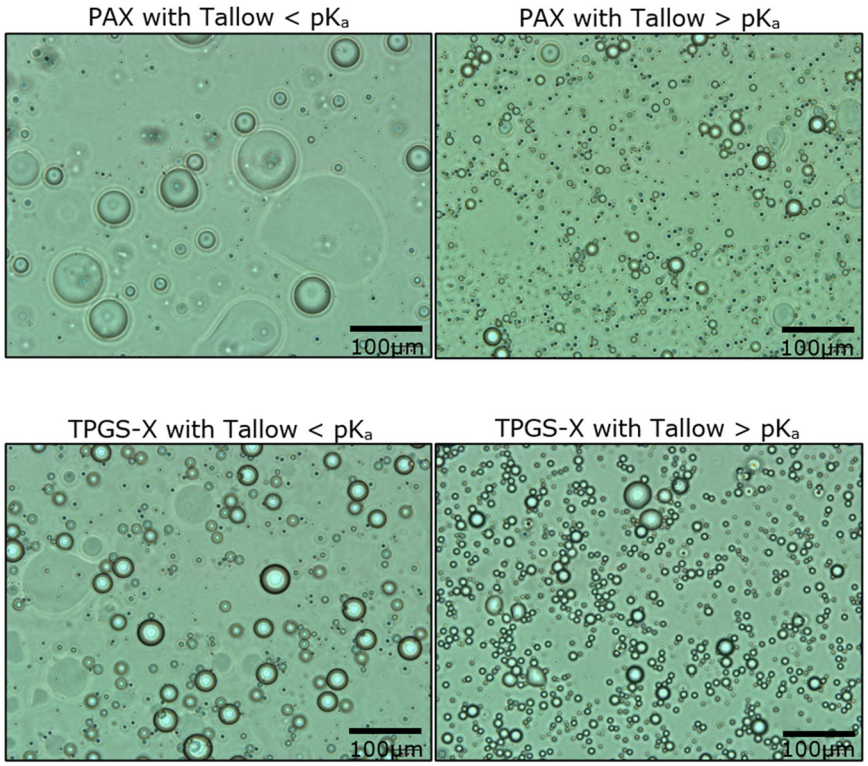

Fig. 5 Optical microscopy images of the kerosene-in-water emulsions within 6 min after the emulsification. PAX with tallow diamine $<$ pK_a and PAX with tallow diamine $>$ pK_a indicate the emulsions with PAX and tallow diamine at pH values below and above the pK_a of tallow diamine, respectively. TPGS-X with tallow diamine $<$ pK_a and TPGS-X with tallow diamine $>$ pK_a show the emulsions with TPGS-X and tallow diamine at pH values below and above the pK_a of tallow diamine, respectively.

that the protonation of the tallow diamine has a strong influence on the stability of the kerosene-in-water emulsion.

However, the emulsions with both xanthates and tallow diamine at pH above the pK_a of tallow diamine remained relatively stable after 10 h. This was because the tallow diamine was mostly deprotonated and, although surface active, did not influence the zeta potential of the droplets. As a result, the zeta potential of such droplets remained negative (−45 to −68 mV) due to the negative charge of the xanthate molecule head groups. Such high negative values of zeta potential induce a strong repulsive force between droplets, even at high ionic strengths. Furthermore, after 100 h, the kerosene-in-water emulsion with PAX above the pK_a of tallow diamine had almost a complete oil phase separation. In contrast, the kerosene-in-water emulsion with the TPGS-X had no oil phase separation even after 100 h.

The creaming rates and oil phase separations from the emulsions below the pK_a of tallow diamine are reported in Fig. 6 while those of the emulsions at pH values above the surfactant pK_a for 100 h are shown in Fig. 6B. The results showed that the protonation of the tallow diamine led to comparatively fast creaming rates and oil phase separation of the emulsions (Fig. 6). This was because the positively charged amine group of the tallow diamine interacted with the negatively charged xanthate at the kerosene–water interface, which resulted in near-zero zeta potential, no EDL repulsion, and low stability of the emulsion. However, at pH values above the pK_a of tallow diamine, the surfactant was mostly deprotonated. As such, there was no interaction between the oil-soluble and water-soluble surfactants, leading to slow creaming rates and minimal oil phase separation, with the xanthates stabilizing the emulsions (Fig. 6B). In addition, at pH values above the pK_a of tallow diamine, the kerosene-in-water emulsion with PAX and tallow diamine exhibited oil phase separation, while there was no oil phase separation from the emulsion with the TPGS-X and tallow diamine. These results are similar to those of the emulsions with only xanthates as the emulsifiers.[41] Moreover, these measurements support our hypothesis that the tallow diamine should be mostly deprotonated for oil attachment to chalcopyrite *via* the xanthate and mostly protonated for oil spreading to the quartz by altering the pH of the aqueous solutions.

Oil contact angle measurements

The concentration of PAX (1.8 mM or 0.04 wt%) in the emulsion formulation was used as the baseline for the experiment. 10% of the concentration (0.18 mM or 0.004 wt%) was selected to understand oil wettability variation with a change in PAX concentration. The same weight percent of the TPGS-X (0.03 mM or 0.004 wt%) was chosen to compare its performance with the same weight percent of PAX. Then, a lower concentration of TPGS-X (0.01 mM or 0.001 wt%) was used to investigate the change in oil wettability with the

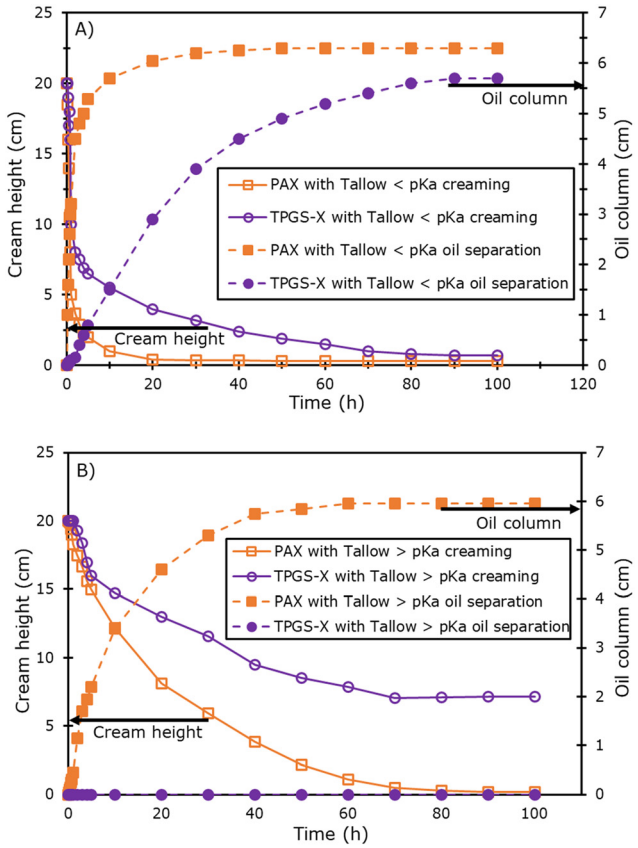

Fig. 6 A) The behaviors of kerosene-in-water emulsions below the pK_a of tallow diamine as a function of time for 100 h. PAX with tallow diamine < pK_a creaming (open squares-orange) and PAX with tallow diamine < pK_a oil separation (filled squares-orange) indicate the creaming rate and oil separation from the emulsions with PAX and tallow diamine at pH values below the pK_a of tallow diamine, respectively. TPGS-X with tallow diamine < pK_a creaming (open circles-purple) and TPGS-X with tallow diamine < pK_a oil separation (filled circles-purple) show the creaming rate and oil separation from the emulsions with TPGS-X and tallow diamine at pH values below the pK_a of tallow diamine, respectively. B) The behaviors of kerosene-in-water emulsions above the pK_a of tallow diamine as a function of time for 100 h. PAX with tallow diamine > pK_a creaming (open squares-orange) and PAX with tallow diamine > pK_a oil separation (filled squares-orange) indicate the creaming rate and oil separation from the emulsions with PAX and tallow diamine at pH values above the pK_a of tallow diamine, respectively. TPGS-X with tallow diamine > pK_a creaming (open circles-purple) and TPGS-X with tallow diamine > pK_a oil separation (filled circles-purple) show the creaming rate and oil separation from the emulsions with TPGS-X and tallow diamine at pH values above the pK_a of tallow diamine, respectively.

surfactant concentration. The concentrations of PAX and TPGS-X used in this study are significantly lower than the critical micelle concentration of the molecules. If PAX forms micelles at all,[45] its critical micelle concentration (CMC) should be at least 100 mM based on results from other linear alkyl xanthates.[56,57] On the other hand, the CMC of TPGS-X is expected to be similar to TPGS with PEG 400, which is between 1.5 mM and 3 mM.[58,59] It is likely that some free xanthate surfactant in the solution may adsorb onto the chalcopyrite as individual molecules before the oil droplet contacts the surface.

Pure kerosene oil droplets in xanthate solutions

The oil contact angles on quartz surfaces (samples C and D in Fig. 2) in water (containing 0.01 M KCl) and aqueous solutions of PAX and TPGS-X with pure kerosene are provided in Fig. 7A. The contact angle measurement on chalcopyrite and quartz surfaces with pure kerosene in water (containing 0.01 M KCl) was used as a blank control to understand the surface hydrophobicity of the mineral surfaces prior to the addition of the surfactants. The mean value of the oil contact angles on the quartz surface in water was approximately 174°, indicating that the quartz surface is naturally very hydrophilic. However, the addition of PAX or TPGS-X reduced the oil contact angle on the quartz surface to 113° with 1.8 mM of PAX and 149° with 0.03 mM of TPGS-X. The oil droplet slightly spread on the quartz surface, but the mineral surface was still relatively hydrophilic as the oil contact angle was well above 90°. The average values and standard deviations of the oil contact angles with pure kerosene are provided in Table S1 in the SI section.

On the other hand, the oil contact angle on the chalcopyrite surfaces (samples A and B in Fig. 2) in water was approximately 88°, indicating that it is oleophilic (hydrophobic) (Fig. 7B). This result indicates that the pure kerosene droplet wets and spreads more on chalcopyrite than on the quartz surface. The addition of PAX and TPGS-X improved the oil wettability on the chalcopyrite surface (49° for 1.8 mM PAX; 37° for 0.03 mM TPGS-X). These results showed that the TPGS-X enhanced the oil wettability more than PAX, even at a lower dosage. This suggests that the TPGS-X is a better hydrophobicity modifier than PAX, as reported in our previous paper.[46] In addition to being a better emulsion stabilizer,[41] which is consistent with TPGS-X HLB of 9.1, and a characteristic of wetting and spreading agents.[60] The average values and standard deviations of the oil contact angle measurements with pure kerosene are provided in Table S2 in the SI section.

Tallow diamine in kerosene oil droplets in xanthate solutions

Oil contact angles on pure minerals. The oil contact angles on quartz surfaces with 0.86 mg g^{-1} tallow diamine in kerosene solution as the drop phase and xanthate solution as the aqueous phase, above and below the pK_a of tallow diamine are provided in Fig. 8. At pH values above the pK_a of the tallow diamine, the oil contact angles were significantly higher than 90° (131° for 1.8 mM PAX; 146° for 0.03 mM TPGS-X), indicating that the oil droplet did not wet the quartz surface when the tallow diamine was mostly deprotonated. The measured values are quite close to those reported for the systems with pure kerosene and xanthates (113° for 1.8 mM PAX; 150° for 0.03 mM TPGS-X). This signifies that at this pH value, the tallow diamine was mostly deprotonated and did not adsorb onto the solid surface. The oil wettability was also not influenced by the negatively charged xanthates since they also do not adsorb onto the negatively charged quartz surface. However, when the tallow diamine was mostly

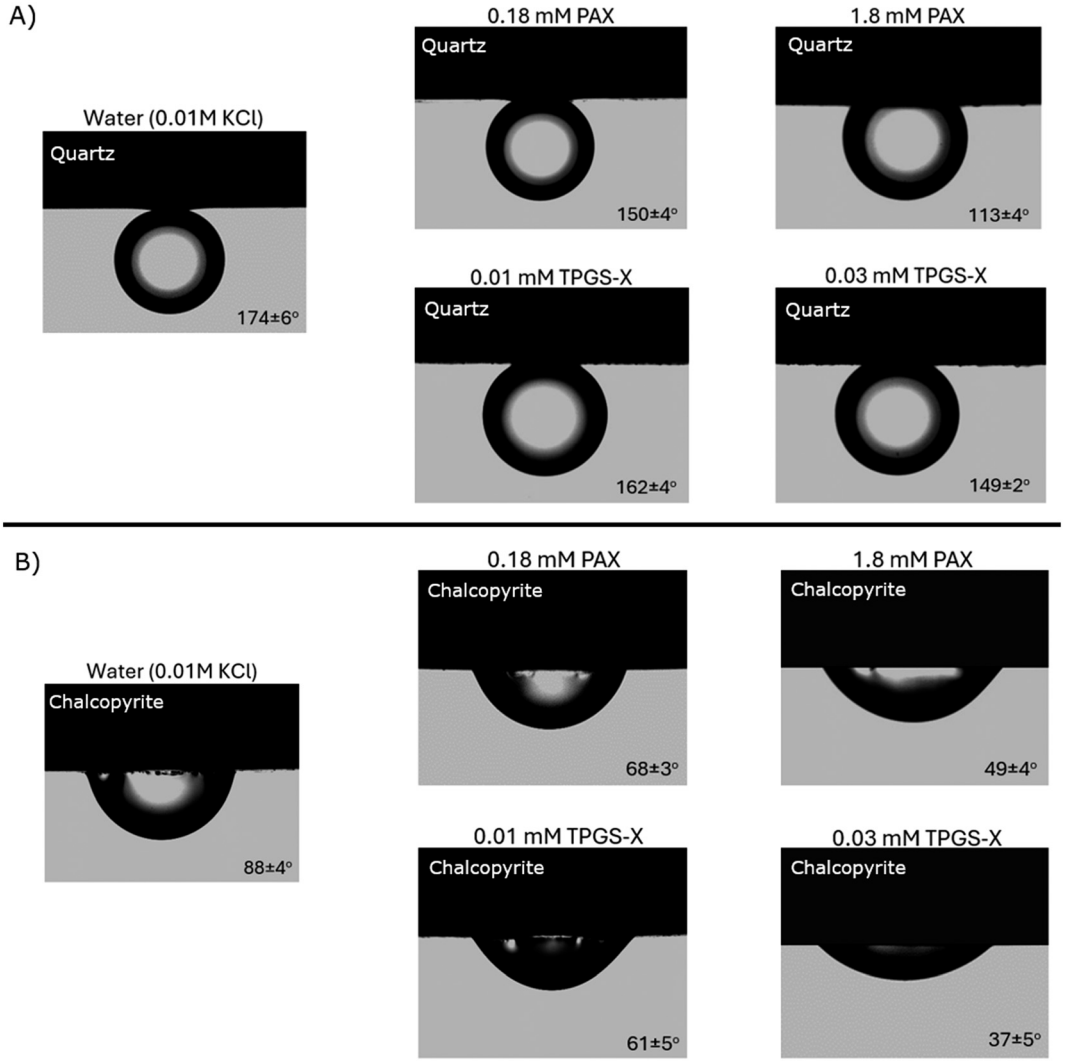

Fig. 7 A). Examples of pure kerosene contact angles on quartz surfaces (samples C and D in Fig. 2) in water and aqueous xanthate solutions. Values are the mean and standard deviation of (n = 8) measurements recorded at different points on the mineral surface. B). Examples of pure kerosene contact angles on chalcopyrite surface (samples A and B in Fig. 2) in water and aqueous xanthate solutions. Values are the mean and standard deviation of (n = 8) measurements recorded at different points on the mineral surface.

protonated at pH values less than the pK_a, the oil contact angles were significantly less than 90° (24° for PAX; 52° for TPGS-X), demonstrating that the tallow diamine adsorbs on to the quartz surface and enables the oil droplet to spread on the quartz surface as reported in Fig. 8. The average values and standard deviations of the oil contact angle measurements with 0.86 mg g^{-1} tallow diamine in kerosene solutions as the drop phase are provided in Table S3.

Furthermore, the oil contact angles on chalcopyrite surfaces with 0.86 mg g^{-1} tallow diamine in kerosene solution as the drop phase and xanthate solution as the aqueous phase, above and below the pK_a of tallow diamine are provided in Fig. 9. These values were less than 90° (49° for 1.8 mM PAX; 39° for 0.03 mM TPGS-X above the pK_a of tallow diamine and 62° for 1.8 mM PAX; 51° for 0.03 mM TPGS-X below the pK_a of tallow diamine). This indicated that the oil wets the chalcopyrite surface regardless of the protonation of the tallow diamine, as the mineral surface exhibited a degree of natural hydrophobicity after polishing.

However, the values are slightly higher when the tallow diamine is mostly protonated, suggesting that the cationic tallow diamine and the anionic xanthate surfactants might be interacting in the system. The tallow diamine likely complexes some of the xanthate, rendering it less likely to adsorb to the chalcopyrite surface, thereby making the surface less oleophilic and slightly increasing the oil contact angle. It was also interesting to note that the measured values (above the pK_a of tallow diamine) are quite close to those observed for the systems with pure kerosene and xanthates (49° for 1.8 mM PAX; 37° for 0.03 mM TPGS-X). This suggests that when the tallow diamine was mostly deprotonated, the oil wettability was influenced only by the xanthates. The average values and standard deviations of the oil contact angle measurements with 0.86 mg g^{-1} tallow

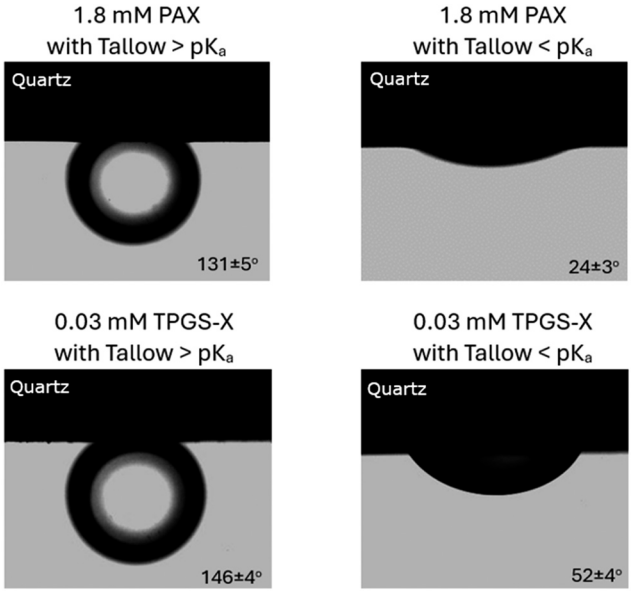

Fig. 8 Examples of 0.86 mg g^{-1} tallow diamine in kerosene solution contact angles on quartz surface (samples C and D in Fig. 2) in aqueous xanthate solutions. Values are the mean and standard deviation of (n = 8) measurements recorded at different points on the mineral surface.

diamine in kerosene solutions as the drop phase are provided in Table S4. Fig. 8 and 9 demonstrate that the oil droplet spreads on quartz but not on chalcopyrite when the pH of the solution is dropped from above to below the pK_a of tallow diamine.

Oil contact angles on composite minerals. Finally, the oil wetting and spreading on composite mineral surfaces (samples E and F in Fig. 2) with 0.86 mg g^{-1} tallow diamine in kerosene solutions as the drop phase and either 1.8 mM PAX or 0.03 mM TPGS-X aqueous solution as the aqueous phases at pH values above and below the pK_a of tallow diamine was investigated. The purpose of these experiments was to determine if the oil could spread from chalcopyrite to quartz by changing the pH. The results are illustrated in Fig. 10A and B, and the videos of the oil wetting and spreading are reported in the SI. At pH values above the pK_a of the tallow diamine, the oil droplet did not spread on the composite sample E (*i.e.*, oil contact angle ≈171° for PAX and 159° for TPGS-X) because the droplet was attached to the quartz patch on sample E. In contrast, the droplet spread on the composite sample F (*i.e.*, oil contact angle ≈64° for PAX and 35° for TPGS-X) because the droplet was attached to the chalcopyrite patch on sample F. Subsequently, a change in solution pH to below the surfactant pK_a enables the oil droplet to spread significantly more on both samples (*i.e.*, oil contact angle ≈9° for PAX and 21° for TPGS-X on sample E; oil contact angle ≈12° for PAX and <10° for TPGS-X on sample F).

This suggests that the droplet on composite mineral E wets and spreads on the quartz when the pH is dropped. This shows that the spreading of oil on a pure quartz particle is possible in the case that all the oil droplets are not already attached to chalcopyrite surfaces before the pH is changed. For this reason, the dosage of the emulsion needs to be carefully controlled to ensure that there are no excess droplets in the system to improve both mineral grade and recovery in the application of the proposed system for composite mineral flotation. In the case of composite mineral F, the results suggest that the droplet is spreading from a chalcopyrite patch to a quartz patch because if the drop remained on the chalcopyrite patch only, it would not spread upon a decrease in the solution pH as demonstrated in Fig. 11. As clearly shown in the videos in the SI section, the oil spreads relatively quickly, which is accompanied by a significant decrease in the oil contact angle. It can also be seen in the videos that the oil droplet sometimes shifts slightly on the surface, as the interaction of tallow diamine and quartz drags and spreads the droplet across a larger area. It should also be noted that there is no visible detachment of the oil droplet from the surface. The average values and standard deviations of the oil contact angle measurements are provided in Table S5 for 1.8 mM PAX and Table S6 for 0.03 mM TPGS-X.

To compare and confirm that this spreading is due to the movement of the oil droplet onto the quartz in a heterogeneous composite surface, a control example was conducted with pure chalcopyrite. Fig. 11A and B show examples of a pure chalcopyrite surface with 0.86 mg g^{-1} tallow diamine in kerosene solutions as the drop phase with 1.8 mM PAX and 0.03 mM TPGS-X solutions as the aqueous phases, respectively. Initially, the xanthate solutions were at pH values above the pK_a of tallow diamine, then the pH was decreased by adding acid. The droplet did not further spread because there are no quartz patches on the pure chalcopyrite sample. The average values and standard deviations of the oil

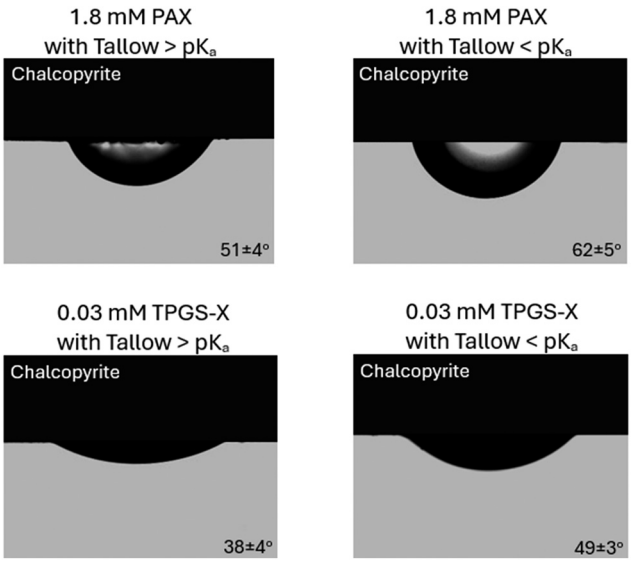

Fig. 9 Examples of 0.86 mg g^{-1} tallow diamine in kerosene solutions contact angles on chalcopyrite surface (samples A and B in Fig. 2) in aqueous xanthate solutions. Values are the mean and standard deviation of (n = 8) measurements at different points on the mineral surface.

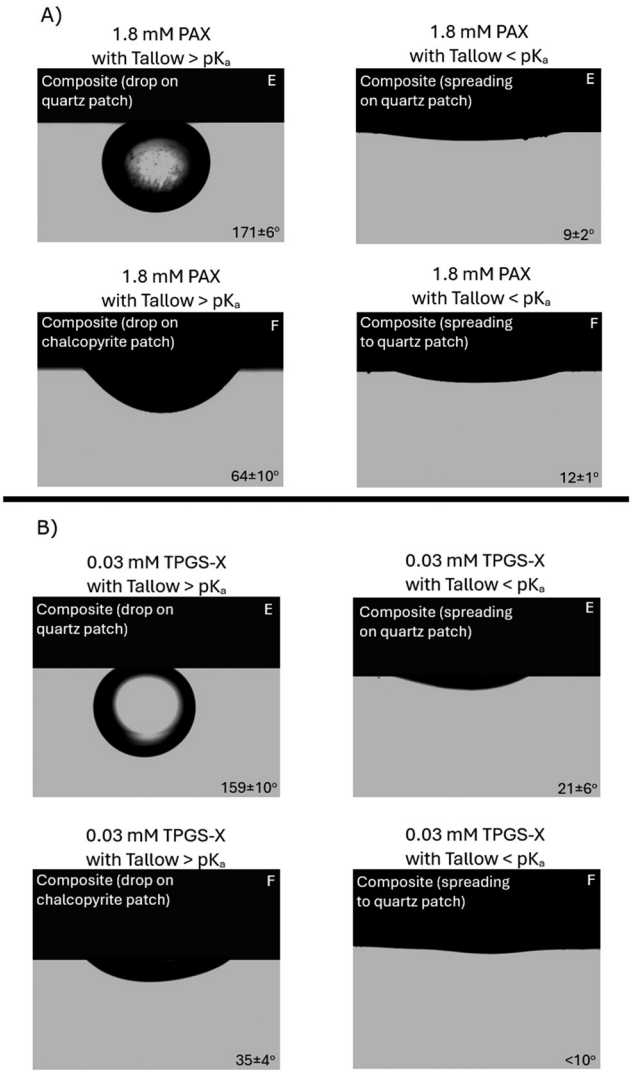

Fig. 10 Examples of 0.86 mg g^{-1} tallow diamine in kerosene solutions contact angles on the composite mineral surface (samples E and F in Fig. 2) in aqueous xanthate solutions. A) PAX. B) TPGS-X. The top two panels show the droplet initially on a quartz patch (left) at pH values above the pK_a of tallow diamine. Upon addition of drops of acid to decrease the pH values to below the pK_a of tallow diamine, the droplet wets and spreads on the quartz (top right). The bottom two panels show the droplet initially on a chalcopyrite patch (left). Upon addition of drops of acid to decrease the pH values to below the pK_a of tallow diamine, the droplet spreads from the chalcopyrite to the quartz (bottom right). Values are the mean and standard deviation of (n = 3) measurements recorded at different points on the mineral surface.

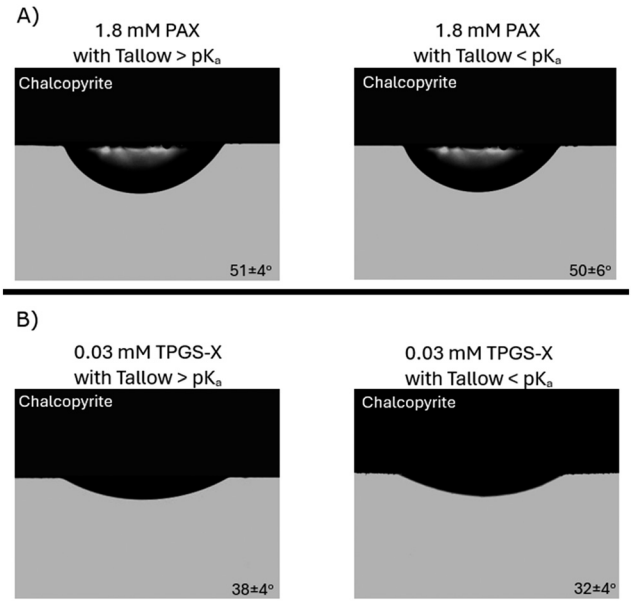

Fig. 11 Examples of 0.86 mg g^{-1} tallow diamine in kerosene solutions contact angles on pure chalcopyrite in aqueous xanthate solutions. A) PAX. B) TPGS-X. The right panel shows the droplet initially on chalcopyrite at pH values above the pK_a of tallow diamine. As shown on the right panel, approximately 9 min after the addition of a few drops of acid to decrease the pH values to below the pK_a of tallow diamine, the oil wettability is not significantly affected. Values are the mean and standard deviation of (n = 3) measurements recorded at different points on the mineral surface.

contact angle measurements are provided in Table S7. The videos of the oil wetting and spreading are reported in the SI.

These results suggest that oil-containing hydrophobicity modifiers can be used for the controlled spreading of oil from chalcopyrite to quartz surfaces. By delivering oil droplets to chalcopyrite-containing particles *via* the selective adhesion facilitated by the xanthates, followed by a decrease in solution pH to facilitate the spreading of the oil droplet to quartz on the composite mineral surface, the hydrophobicity of the entire particle will be increased. It is expected that the improved hydrophobicity of the composite particle surface would minimize the detachment of coarse particles from air bubbles in the conventional flotation cell. This should ultimately improve the recovery of coarse composite chalcopyrite–quartz particles in froth flotation. Further studies on the application of the novel system for coarse particle flotation are currently underway and are intended to be submitted later this year.

Conclusion

The stability of the kerosene-in-water emulsion is dependent on the protonation of the tallow diamine. The emulsion was relatively stable when the tallow diamine was mostly deprotonated because the tallow diamine did not influence the negative charge on the xanthates, which acted to stabilize the emulsions. However, when the tallow diamine was mostly protonated, the emulsion was unstable due to the interaction between the positively charged amine group of the tallow diamine and the negatively charged xanthates, reducing the zeta potential of the oil–water interface to 0 mV, leading to unstable emulsions. The oil wettability of pure kerosene on chalcopyrite (oil contact angle of 88°) was greater than that on quartz (oil contact angle of 174°) because chalcopyrite is weakly hydrophobic, whereas quartz is hydrophilic. Xanthates enhanced oil wettability on chalcopyrite but not on quartz. However, α-tocopherol polyethylene glycol 400 succinate

xanthate (TPGS-X) decreased the contact angle on chalcopyrite to a greater extent at a lower concentration than potassium amyl xanthate (PAX). The addition of tallow diamine to the oil phase improved the oil wettability on the quartz surface only when it was mostly protonated at a pH value lower than the pK_a of tallow diamine. The addition of tallow diamine to the oil phase had little influence on the wetting of chalcopyrite either above or below the pK_a of tallow diamine. After the initial contact of droplets to composite mineral surfaces composed of patches of both chalcopyrite and quartz, changing the pH value from above to below the pK_a of tallow diamine facilitated the spreading of the oil both on the quartz and from the chalcopyrite to quartz. These results show that oil-containing hydrophobicity modifiers can improve the surface hydrophobicity of composite chalcopyrite–quartz minerals. Further studies are underway to apply the proposed system for the froth flotation of coarse composite chalcopyrite–quartz ores to improve the recovery of copper minerals.

Author contributions

Azeez G. Aregbe: investigation, conceptualization, formal analysis, data curation, methodology, writing – original draft, writing – review and editing. Wei Sung Ng: investigation, formal analysis, methodology, writing – review and editing. Tina Hsia: investigation, methodology, writing – review and editing. Anton Blencowe: investigation, formal analysis, methodology, resources, supervision, writing – review and editing. Alireza Allahyari: investigation, formal analysis, methodology, writing – review and editing. Marta Krasowska: conceptualization, methodology, resources, supervision, funding acquisition, writing – review and editing. San H. Thang: conceptualization, methodology, resources, supervision, funding acquisition, writing – review and editing. George V. Franks: formal analysis, conceptualization, methodology, project administration, resources, supervision, funding acquisition, writing – review and editing.

Conflicts of interest

There are no conflicts to declare.

Data availability

The data supporting this article have been included as part of the supplementary information (SI). Supplementary information is available. See DOI: https://doi.org/10.1039/d5lf00275c.

Acknowledgements

The authors would like to thank Professor Ray Dagastine for helpful discussions regarding emulsion stability and contact angle measurement. Thanks to Prof. David Beattie for helping frame the research project. Thanks to Prof. Peter Scales and Yuxuan Luo for suggesting tallow diamine. Thanks to Piotr Pawliszak for helpful discussions on visual analysis of contact angle measurements and Cintya Dharmayanti for help with NMR experiments. The authors acknowledge the funding support from the Australian Research Council for the ARC Centre of Excellence for Enabling Eco-Efficient Beneficiation of Minerals, grant number CE200100009. This work was performed in part at the Materials Characterisation and Fabrication Platform (MCFP) at the University of Melbourne and the Victorian Node of the Australian National Fabrication Facility (ANFF). The authors also acknowledge the technical staff of the University of Melbourne MCFP (Materials Characterisation & Fabrication Platform) for equipment access and training.

References

1 N. M. Kovalchuk and M. J. H. Simmons, Surfactant-mediated wetting and spreading: recent advances and applications, *Curr. Opin. Colloid Interface Sci.*, 2021, **12**, 101375.
2 Z. Zhu, Y. Jiang and J. W. Drelich, Droplet spreading and adhesion on spherical surfaces, *Langmuir*, 2022, **38**, 8456–8461.
3 Q. Wang and H. Wang, Fabrication of textured surface with controllable wettability via laser-thermal hybrid processing, *Mater. Lett.*, 2022, **315**, 131954.
4 Z. Huangfu, W. Sun, H. Zhang, C. Chen and C. Zhang, Hydrophilic modification of macroscopically hydrophobic mineral talc and its specific application in flotation, *Langmuir*, 2024, **40**, 25988–25996.
5 G. McHale, R. Ledesma-Aguilar and C. Neto, Cassie's law reformulated: composite surfaces from superspreading to superhydrophobic, *Langmuir*, 2023, **39**, 11028–11035.
6 S. Mitra, A. Kim, B. Zhao and S. K. Mitra, Rapid spreading of yield-stress liquids, *Langmuir*, 2024, **40**, 18968–18976.
7 A. Møller, A. Beheshti, W. Skinner, G. Franks, D. Beattie and M. Krasowska, Hydrophobic surfaces in mineral flotation: the effect of (physical and chemical) heterogeneity on wettability and wetting film stability, *Encyclopedia Solid-Liquid Interface*, 2024, pp. 494–504.
8 H.-J. Butt, K. Graf and M. Kappl, *Physics and chemistry of interfaces*, John Wiley & Sons, 2003.
9 T. Sun, G. Wang, L. Feng, B. Liu, Y. Ma, L. Jiang and D. Zhu, Reversible switching between superhydrophilicity and superhydrophobicity, *Angew. Chem., Int. Ed.*, 2004, **43**, 357–360.
10 K. Ichimura, S. Oh and M. Nakagawa, Light-driven motion of liquids on a photoresponsive surface, *Science*, 2002, **298**, 1624–1626.
11 J. Lahann, S. Mitragotri, T. Tran, H. Kaido, J. Sundaram, I. S. Choi, S. Hoffer, G. A. Somorjai and R. Langer, A reversibly switching surface, *Science*, 2003, **299**, 371–374.
12 D. Crevoisier, P. Fabre, J. Corpart and L. Leibler, Switchable tackiness and wettability of a liquid crystalline polymer, *Science*, 1999, **285**, 1246–1249.
13 S. Minko, M. Müller, M. Motornov, M. Nitschke, K. Grundke and M. Stamm, Two-level structured self-adaptive surfaces with reversibly tunable properties, *J. Am. Chem. Soc.*, 2003, **125**, 3896–3900.

14 M. Ali, Y. Yang, A. Abdoh and Y. Mohammed, Topographical characteristics of 3D printed polymeric microneedle surface and its impact on coating formulation attributes, *RSC Appl. Interfaces*, 2024, **1**, 1108.
15 Q. Yang, M. E. Woods and R. Gakhar, Wettability studies of LiCl-KCl and FLiNaK on metal and non-metal substrates, *RSC Appl. Interfaces*, 2025, **2**, 715–723.
16 K. Yeadon, E. P. C. Lai, X. Huang and N. Song, Influence of surface roughness and metal oxide nanoparticles on airframe with icephobic coatings, *RSC Appl. Interfaces*, 2025, **2**, 82.
17 S. Yang and R. Pelton, Nanoparticle flotation collectors II: The role of nanoparticle hydrophobicity, *Langmuir*, 2011, **27**(18), 11409–11415.
18 B. B. Said, M. Rudolph, D. Ebert, D. Goldmann and L. Pereira, Nanoparticle depressants in froth flotation – The effect of colloidal silica with different size and surface modifications on the selective separation of semi-soluble salt type minerals, *Colloids Surf., A*, 2024, **690**, 133697.
19 P. B. Kowalczuk, O. Sahbaz and J. Drzymala, Maximum size of floating particles in different flotation cells, *Miner. Eng.*, 2011, **24**, 766–771.
20 W. J. Trahar and L. J. Warren, The flotability of very fine particles – A review, *Int. J. Miner. Process.*, 1976, **3**, 103–131.
21 S. J. Anzoom, G. Bournival and S. Ata, Coarse particle flotation: A review, *Miner. Eng.*, 2024, **206**, 108499.
22 K. L. Sutherland, Physical chemistry of flotation XI, Kinetics of the flotation process, *J. Phys. Colloid Chem.*, 1948, **52**(2), 394–425.
23 S. Farrokhpay, L. Filippov and D. Fornasiero, Flotation of fine particles: A review, *Miner. Process. Extr. Metall. Rev.*, 2020, **42**(7), 473–483.
24 S. Ata and G. J. Jameson, Recovery of coarse particles in the froth phase – A case study, *Miner. Eng.*, 2013, **45**, 121–127.
25 B. Awatey, W. Skinner and M. Zanin, Effect of particle size distribution on recovery of coarse chalcopyrite and galena in Denver flotation cell, *Can. Metall. Q.*, 2013, **52**(4), 465–472.
26 S. Gautam and G. J. Jameson, The detachment of particles from bubbles at various locations in a turbulent flotation cell, *Miner. Eng.*, 2019, **132**, 316–325.
27 J. Kohmuench, M. Mankosa, H. Thanasekaran and A. Hobert, Improving coarse particle flotation using the HydroFloat™ (raising the trunk of the elephant curve), *Miner. Eng.*, 2018, **121**, 137–145.
28 G. J. Jameson and C. Emer, Coarse chalcopyrite recovery in a universal froth flotation machine, *Miner. Eng.*, 2019, **134**, 118–133.
29 J. Gao, X. Bu, S. Zhou, X. Wang, M. Alheshibri, Y. Peng and G. Xie, Graphite flotation by β-cyclodextrin/kerosene pickering emulsion as a novel collector, *Miner. Eng.*, 2022, **178**, 107412.
30 X. Ma, L. Xia, S. Wang, H. Zhong and H. Jia, Structural modification of xanthate collectors to enhance the flotation selectivity of chalcopyrite, *Ind. Eng. Chem. Res.*, 2017, **56**, 6307–6316.
31 J. Xiao, G. Liu, H. Zhong, Y. Huang and Z. Cao, The flotation behavior and adsorption mechanism of o-isopropyl-s-[2-(hydroxyimino) propyl] dithiocarbonate ester to chalcopyrite, *J. Taiwan Inst. Chem. Eng.*, 2017, **71**, 38–46.
32 W. Wang, X. Ma, Q. Lin, H. Zhong, Z. Gao and S. Wang, A green flotation collector towards the efficient separation of chalcopyrite from pyrite with high selectivity, *Miner. Eng.*, 2023, **201**, 108227.
33 W. C. Simpson, R. L. Griffin and T. K. Miles, Relationship of asphalt properties to the chemical constitution, *J. Chem. Eng. Data*, 1961, **6**, 426–429.
34 J. L. Gorman, R. J. Crawford and I. H. Harding, Bitumen emulsions in road construction - A review, *Aust. Road Res.*, 2004, **13**(1), 25–38.
35 A. Al-Mohammedawi and K. Mollenhauer, Current research and challenges in bitumen emulsion manufacturing and its properties, *Materials*, 2022, **15**(6), 2026.
36 M. Hwang, Y. Mu, L. Cao and Y. Peng, The influence of NaCl on xanthate adsorption on chalcopyrite surface and chalcopyrite flotation, *Miner. Eng.*, 2024, **218**, 109026.
37 S. Chander, Electrochemistry of sulfide mineral flotation, *Min. Metall. Explor.*, 1988, **5**, 104–114.
38 Y. Zhang, Z. Cao, Y. Cao and C. Sun, FTIR studies of xanthate adsorption on chalcopyrite, pentlandite and pyrite surfaces, *J. Mol. Struct.*, 2013, **1048**, 434–440.
39 *Handbook of Detergents, Part C: Analysis, Surfactant science series*, ed. H. Waldhoff and R. Spilker, CRC Press, 2016.
40 A. Vidyadhar, K. H. Rao and K. S. E. Forssberg, Adsorption of N-tallow 1,3-propanediamine–dioleate collector on albite and quartz minerals, and selective flotation of albite from greek stefania feldspar ore, *J. Colloid Interface Sci.*, 2002, **248**, 19–29.
41 A. G. Aregbe, T. Hsia, M. Krasowska, S. H. Thang and G. V. Franks, Stability and characteristics of kerosene-in-water emulsions with xanthate surfactants: Influence of hydrophilic-lipophilic balance and molecular weight, *Colloids Surf., A*, 2024, **700**, 134818.
42 Q. Lin, J. Yang, J. Wang, J. Wang, S. Wang, X. Ma and H. Zhong, Water-bridged self-assembly of low-odor xanthate surfactant for selective flotation of chalcopyrite, *J. Mol. Liq.*, 2024, **398**, 124246.
43 J. A. Mielczarski, E. Mielczarski and J. M. Cases, Interaction of amyl xanthate with chalcopyrite, tetrahedrite, and tennantite at controlled potentials. Simulation and spectroelectrochemical results for two-component adsorption layers, *Langmuir*, 1996, **12**(26), 6521–6529.
44 L. Bach, R. D. Norregard, V. Hansen and K. Gustavson, *Review on environmental risk assessment of mining chemicals used for mineral separation in the mineral resources industry and recommendations for Greenland*, Aarhus University, DCE-Danish Centre for Environmental and Energy, 2016.
45 M. A. Elizondo-Alvarez, A. Uribe-Salas and S. Bello-Teodoro, Chemical stability of xanthates, dithiophosphinates, and hydroxamic acids in aqueous solutions and their environmental implications, *Ecotoxicol. Environ. Saf.*, 2011, **207**, 111509.

46 A. G. Aregbe, W. S. Ng, T. Hsia, S. H. Thang and G. V. Franks, A novel vitamin E-based xanthate collector for chalcopyrite-quartz mineral flotation, *Sep. Purif. Technol.*, 2025, **378**(Part 2), 134714.
47 W. C. Griffin, Calculation of HLB values of non-ionic surfactants, *J. Soc. Cosmet. Chem.*, 1954, **5**(4), 249–256.
48 C. D. LaSusa, Marketing and economics of oleochemicals to the oil patch, *J. Am. Oil Chem. Soc.*, 1984, **61**(2), 184–187.
49 D. Jero, N. Causse, O. Marsan, T. Buffeteau, F. Chaussec, A. Buvignier, M. Roy and N. Pebere, Film-forming amines adsorption and corrosion kinetics on carbon steel surface in neutral solution investigated by eis and pm-irras analysis, *Electrochim. Acta*, 2024, **443**, 141925.
50 M. A. Soldatov, V. M. Nosova, E. A. Monin and P. A. Storozhenko, Use of reversed-phase HPLC for the qualitative and quantitative control of the production of n-octadecyl-1,3-diaminopropane, *J. Anal. Chem.*, 2019, **74**(2), 121–125.
51 Y. Shen, D. R. Nagaraj, R. Farinato and P. Somasundaran, Study of xanthate decomposition in aqueous solutions, *Miner. Eng.*, 2016, **93**, 10–15.
52 J. Saien and V. Fadaei, The study of interfacial tension of kerosene-water under influence of CTAB surfactant and different size silica nanoparticles, *J. Mol. Liq.*, 2018, **255**, 439–446.
53 H. Molavi, S. Hosseinpour, H. Bahmanyar and M. Shariaty-Niasar, Investigation on local and average statichold-ups in liquid–liquid systems in arotary disc contactor, *Can. J. Chem. Eng.*, 2011, **89**, 1464–1472.
54 M. P. Shahri, S. R. Shadizadeh and M. Jamialahmadi, Applicability test of new surfactant produced from zizyphus spina-christi leaves for enhanced oil recovery in carbonate reservoirs, *J. Jpn. Pet. Inst.*, 2012, **55**(1), 27–32.
55 A. Aregbe, W. S. Ng and G. Franks, Improving chalcopyrite recovery from coarse copper-gold ore with kerosene, *Conference proceedings at the XXXI IMPC-International Mineral Processing Congress in Washington D.C.*, 2024, pp. 2418–2426.
56 G. Han, S. Su, Y. Huang, W. Peng, Y. Cao and J. Liu, An insight into flotation chemistry of pyrite with isomeric xanthates: A combined experimental and computational study, *Minerals*, 2018, **8**, 166.
57 I. C. Hamilton and R. Woods, Surfactant properties of alkyl xanthates, *Int. J. Miner. Process.*, 1986, **17**, 113–120.
58 M. Sadoqi, C. A. Lau-Cam and S. H. Wu, Investigation of the micellar properties of the tocopheryl polyethylene glycol succinate surfactants TPGS 400 and TPGS 1000 by steady state fluorometry, *J. Colloid Interface Sci.*, 2009, **333**(2), 585–589.
59 P. Y. Ho, T. K. Yeh, H. T. Yao, H. L. Lin, H. Y. Wu, Y. K. Lo, Y. W. Chang, T. H. Chiang, S. H. W. Wu, Y. S. Chao and C. T. Chen, Enhanced oral bioavailability of paclitaxel by D-α-tocopheryl polyethylene glycol 400 succinate in mice, *Int. J. Pharm.*, 2008, **359**, 174–181.
60 S. V. MacWilliams, A. J. Clulow, G. Gillies, A. D. Beattie and M. Krasowska, Recent advances in studying crystallisation of mono-and di-glycerides at oil-water interfaces, *Adv. Colloid Interface Sci.*, 2024, 103138.